

The near-infrared radius-luminosity relationship for active galactic nuclei

Hermine Landt^{1*}†, Misty C. Bentz²†, Bradley M. Peterson^{3,4}, Martin Elvis⁵†, Martin J. Ward⁶†, Kirk T. Korista⁷ and Margarita Karovska⁵

¹*School of Physics, University of Melbourne, Parkville, VIC 3010, Australia*

²*Department of Physics and Astronomy, Georgia State University, 709 One Park Place South, Atlanta, GA 30303, USA*

³*Department of Astronomy, The Ohio State University, 140 West 18th Avenue, Columbus, OH 43210, USA*

⁴*Center for Cosmology and AstroParticle Physics, The Ohio State University, 191 West Woodruff Avenue, Columbus, OH 43210, USA*

⁵*Harvard-Smithsonian Center for Astrophysics, 60 Garden Street, Cambridge, MA 02138, USA*

⁶*Department of Physics, University of Durham, South Road, Durham, DH1 3LE*

⁷*Department of Physics, Western Michigan University, 1903 W. Michigan Avenue, Kalamazoo, MI 49008, USA*

Accepted . Received ; in original form

ABSTRACT

Black hole masses for samples of active galactic nuclei (AGN) are currently estimated from single-epoch optical spectra. In particular, the size of the broad-line emitting region needed to compute the black hole mass is derived from the optical or ultraviolet continuum luminosity. Here we consider the relationship between the broad-line region size, R , and the near-infrared (near-IR) AGN continuum luminosity, L , as the near-IR continuum suffers less dust extinction than at shorter wavelengths and the prospects for separating the AGN continuum from host-galaxy starlight are better in the near-IR than in the optical. For a relationship of the form $R \propto L^\alpha$, we obtain for a sample of 14 reverberation-mapped AGN a best-fit slope of $\alpha = 0.5 \pm 0.1$, which is consistent with the slope of the relationship in the optical band and with the value of 0.5 naïvely expected from photoionisation theory. Black hole masses can then be estimated from the near-IR virial product, which is calculated using the strong and unblended Paschen broad emission lines (Pa α or Pa β).

Key words: galaxies: active – galaxies: nuclei – infrared: galaxies – quasars: general

1 INTRODUCTION

The discovery of tight correlations between a galaxy’s central black hole mass and the luminosity and velocity dispersion of its stellar bulge (Magorrian et al. 1998; Gebhardt et al. 2000; Ferrarese & Merritt 2000) is expected to strongly constrain how galaxies form and grow over cosmic time. Therefore, much effort goes in particular into measuring the rate of black hole growth (e.g., Yu & Tremaine 2002; Heckman et al. 2004; Kelly et al. 2009). Since this requires both large samples of galaxies with easily obtainable black hole mass estimates and sources that probe the highest

redshifts, such studies rely heavily on active galactic nuclei (AGN).

In AGN, black hole masses can be readily estimated from single-epoch optical spectra. Assuming that the dynamics of the broad-emission line gas seen in these sources is dominated by the gravitational force of the black hole, one can use the virial theorem to calculate black hole masses from only two observables, the velocity dispersion and radial distance of the emitting gas from the central source (e.g., Peterson et al. 2004). The velocity dispersion can be obtained from the widths of the Balmer hydrogen lines (H β or H α) and the continuum luminosity at (rest-frame) 5100 Å serves as a surrogate for the size of the broad-line region (BLR). The latter finds its justification in the work of Peterson (1993), Wandel et al. (1999) and Kaspi et al. (2000), who showed that emission-line lags, and so broad-emission line radii, derived from optical reverberation mapping studies correlate with the optical luminosity (of the ionising component) largely as expected from simple pho-

* E-mail: hlandt@unimelb.edu.au

† Visiting Astronomer at the Infrared Telescope Facility, which is operated by the University of Hawaii under Cooperative Agreement no. NNX-08AE38A with the National Aeronautics and Space Administration, Science Mission Directorate, Planetary Astronomy Program.

Table 1. Reverberation-Mapped Sample of AGN

| Object Name (1) | $R_{H\beta}$ [lt-days] (2) | $\log \nu L_{1\mu m}$ [erg s ⁻¹] (3) | $\log \nu L_{1\mu m}^{AGN}$ [erg s ⁻¹] (4) |
|--------------------|-------------------------------------|--|--|
| 3C273 | 307 ⁺⁶⁹ ₋₉₁ | 45.81±0.02 | 45.64±0.10 |
| Mrk876 | 40±15 | 44.77 | 44.55 |
| PG0844+349 | 32 ⁺¹⁴ ₋₁₃ | 44.28±0.02 | 44.28±0.10 |
| Mrk110 | 26 ⁺⁴ ₋₆ | 43.69±0.08 | 43.66±0.05 |
| Mrk509 | 80 ⁺⁶ ₋₅ | 44.05±0.03 | 44.07±0.04 |
| Ark120 | 40 ⁺⁴ ₋₆ | 44.26±0.06 | 43.70±0.10 |
| Mrk817 | 22 ⁺² ₋₃ | 43.71±0.03 | 43.64±0.01 |
| Mrk290 | 9±1 | 43.43±0.04 | 43.22±0.12 |
| Mrk335 | 16 ⁺³ ₋₄ | 43.49±0.05 | 43.35±0.07 |
| Mrk79 | 15 ⁺³ ₋₅ | 43.30±0.04 | 43.20±0.05 |
| NGC5548 | 18.0 ± 0.6 | 43.12±0.05 | 42.97±0.09 |
| NGC7469 | 4.5 ^{+0.7} _{-0.8} | 43.45 | 43.10 |
| NGC4593 | 3.7±0.8 | 42.73±0.02 | 42.50±0.06 |
| NGC4151 | 7±1 | 42.13±0.06 | 41.84±0.05 |

The columns are: (1) object name; (2) radius of the H β broad-emission line region (in light-days) (H α for PG 0844+349); average integrated 1 μm continuum luminosity (4) as observed and (5) flux-calibrated relative to best-weather epoch and host galaxy-subtracted. Errors represent 1 σ uncertainties. For sources with multiple radius measurements we list the weighted average (in boldface).

toionisation arguments. This correlation is now referred to as the radius-luminosity (R - L) relationship.

We consider here the application of this technique in the near-infrared (near-IR), which potentially affords some advantages over the optical (and ultraviolet). First, the observed optical continuum can be severely contaminated by host galaxy starlight if a large slit is used (as is often the case in reverberation studies), especially in low-redshift sources that have a weak AGN or sources with a luminous stellar bulge, and so does not give directly the ionising flux. High-resolution, deep optical images are then required to estimate the host galaxy starlight enclosed in the aperture in order to correct the optical spectra (Bentz et al. 2006, 2009). Secondly, the optical hydrogen broad-emission lines, in particular H β , are strongly blended with other species, making it difficult to reliably measure the line width. Thirdly, all optical measures can suffer from dust extinction.

Here we present the radius-luminosity relationship in the near-IR, which, in conjunction with the width of the strong and unblended Paschen broad emission lines Pa α and Pa β , can be used to estimate AGN black hole masses. In Section 2, we introduce the data and present the near-IR R - L relationship. Its application is discussed in Section 3. In Section 4, we present our conclusions. Throughout this paper we have assumed cosmological parameters $H_0 = 70$ km s⁻¹ Mpc⁻¹, $\Omega_M = 0.3$, and $\Omega_\Lambda = 0.7$.

2 THE NEAR-INFRARED R - L RELATIONSHIP

We have recently shown (Landt et al. 2011) that in broad-emission line AGN the accretion disc spectrum, which is believed to be the main source of ionising radiation, extends well into the near-IR and still dominates the continuum at

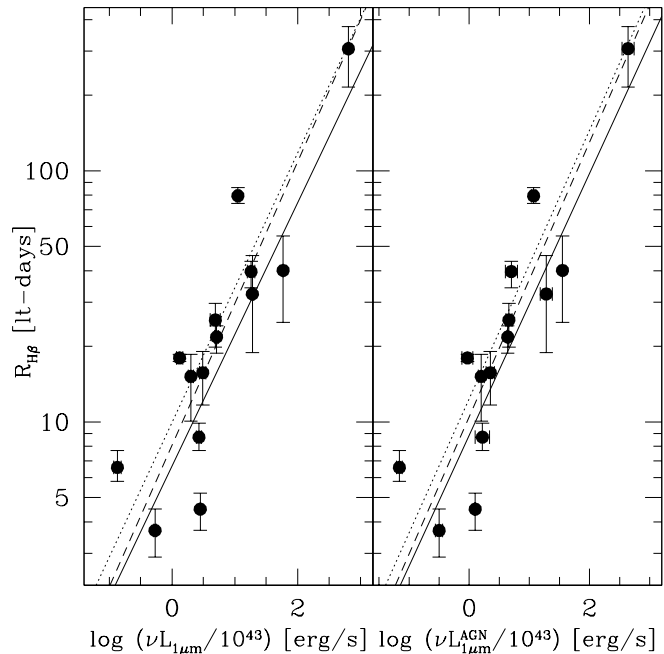


Figure 1. The radius of the H β broad-emission line region (in light-days) versus the average 1 μm continuum luminosity as observed (left panel) and flux-calibrated relative to best-weather epoch and host galaxy-subtracted (right panel). For sources with multiple radius measurements we plot the weighted average. The dashed, solid and dotted lines indicate the correlations obtained with the BCES, FITEXY and GaussFit routines, respectively.

$\sim 1 \mu m$. Therefore, a single-epoch near-IR spectrum can in principle be used to estimate the broad-emission line radius.

In Fig. 1 we verify this conjecture by plotting the radius of the H β broad-emission line region ($R_{H\beta}$) versus the integrated 1 μm continuum luminosity for the reverberation-mapped AGN in our sample (14 objects; see Table 1). Values for the radius of the H β broad-line region are from Bentz et al. (2009) and for Mrk 290 from Denney et al. (2010). The near-IR measures are based on data obtained with the SpeX spectrograph (Rayner et al. 2003) at the NASA Infrared Telescope Facility (IRTF) on Mauna Kea, Hawai'i. The excellent atmospheric seeing at this observing site allowed us to use a relatively narrow slit of 0.8'', which excluded most of the host galaxy starlight. The only exceptions were Mrk 590 and NGC 3227, two reverberation-mapped AGN in our sample that were found to be in a very low state with the continuum strongly dominated by host galaxy emission (see Fig. 6 in Landt et al. 2011). Therefore, they are omitted from the present study. We observed sources on average twice within a period of ~ 3 years (Landt et al. 2008, 2011). Here we use the mean integrated 1 μm continuum luminosity and the error on the mean. We consider both the observed values ($\nu L_{1\mu m}$) and the pure AGN values ($\nu L_{1\mu m}^{AGN}$). The latter were derived by performing a relative flux-calibration using the [S III] $\lambda 9531$ narrow emission line in the best-weather epoch and correcting for host-galaxy starlight using the *Hubble Space Telescope* (HST) images of Bentz et al. (2006, 2009) and for Mrk 290

a recent, unpublished *HST* image (Bentz et al. in prep.). Further details are provided by Landt et al. (2011).

We have performed linear fits of the form $\log R_{H\beta} = K + \alpha \log(\nu L_{\nu}/10^{43})$ following the approach of Bentz et al. (2006) and Bentz et al. (2009). In particular, we have used the three fitting routines BCES (Akritas & Bershady 1996), FITEXY (Press et al. 2007) and GaussFit (McArthur et al. 1994) that can incorporate errors on both variables and, except for GaussFit, allow us to account for intrinsic scatter. Note that accounting for intrinsic scatter has the effect of increasing the weight given to data points with the largest errors, which is preferred if the intrinsic dispersion is larger than the measurement errors (Tremaine et al. 2002). Roughly half of our sample (6/14 sources) has multiple measurements of $R_{H\beta}$ and, therefore, we have considered the following two cases: (i) using the average derived from all measurements for a particular source and weighted by the mean of the positive and negative errors (i.e., weighted averages) and (ii) using Monte-Carlo (MC) techniques to randomly sample $R_{H\beta}$ from the individual values for each object. Two sources have only one epoch of near-IR data and in these cases we have assigned to the logarithmic luminosity the average error of the sample. We obtain significant correlations in all cases. Table 2 lists the results, which are shown for the case of the weighted averages in Fig. 1. Note that the near-IR continuum luminosities and the optical broad-emission line radii are not measured simultaneously, which is expected to increase the scatter in their relationship.

All six cases for both total and AGN $1 \mu\text{m}$ continuum luminosity give similar values for the slope and the intercept. The slope is in most cases $\sim 0.5 \pm 0.1$ and always consistent with a value of 0.5. Simple photoionisation arguments suggest that a given emission line will be produced at the same ionising *flux* in all AGN and therefore $R \propto L^{1/2}$. Our results are similar to the best-fit slope of $0.52^{+0.06}_{-0.07}$ found in the optical by Bentz et al. (2009), who used host galaxy-subtracted fluxes of 34 reverberation-mapped AGN (more than twice our sample size).

3 DISCUSSION

Given the importance of the R - L relationship for AGN black hole mass determinations, alternatives to the optical continuum luminosity are already being explored, e.g., the X-ray luminosity and broad $H\beta$ line luminosity (Kaspi et al. 2005; Greene et al. 2010), the $[\text{O III}] \lambda 5007 \text{ \AA}$ emission-line luminosity (Greene et al. 2010), the $\text{Pa}\alpha$ and $\text{Pa}\beta$ emission-line luminosities (Kim et al. 2010), and the $[\text{Ne V}] \lambda 14.32 \mu\text{m}$ and $[\text{O IV}] \lambda 25.89 \mu\text{m}$ emission-line luminosities (Dasyra et al. 2008; Greene et al. 2010). The $1 \mu\text{m}$ continuum luminosity is an efficient alternative that connects directly to the spectrum of the ionising source.

Near-IR spectroscopy is now available at excellent observing sites that regularly achieve subarcsecond seeing. This means that the host galaxy flux contribution in the near-IR can be reduced to a minimum. For example, a slit width (and seeing) of $0.8''$ in the near-IR relative to one of $3''$, which is typical of most optical telescope sites, leads to a reduction of the extraction aperture (and so of the host galaxy flux contribution, assuming constant surface bright-

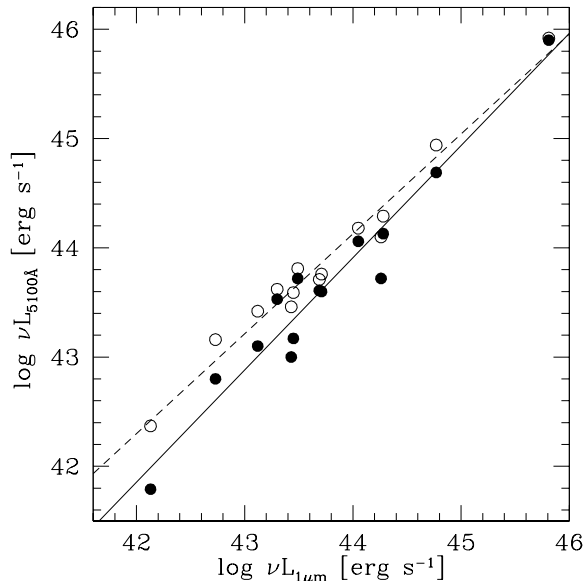


Figure 2. The average integrated 5100 \AA continuum luminosity from Bentz et al. (2009) versus the average integrated $1 \mu\text{m}$ continuum luminosity. Open and filled circles indicate total and host galaxy-corrected optical values, respectively. The host galaxy correction to the optical luminosities has the effect of changing the observed correlation slope from 0.91 ± 0.04 (dashed line) to 1.03 ± 0.07 (solid line).

ness) by a factor of ~ 14 . The case is exacerbated if we consider the much larger apertures employed in optical reverberation studies ($5 - 10''$). Additionally, the seeing is improved at longer wavelengths, thus reducing the extraction aperture further (e.g., by a factor of ~ 1.3 at $1 \mu\text{m}$ relative to 5100 \AA). Adaptive optics should make it possible to realise even greater gains in the near-IR relative to the ground-based optical.

As our results show, the correlations for the total and AGN $1 \mu\text{m}$ continuum luminosity are consistent with each other and so independent of the host galaxy flux subtraction, although the slope is more often ~ 0.5 and the scatter slightly smaller for the latter. Performing the same fits for our sample (14 sources) using the optical data of Bentz et al. (2009) with the host galaxy flux subtracted gives results that are more similar to the total rather than to the AGN near-IR spectra (see Table 2). However, if we consider their entire optical sample (34 sources), we obtain results similar to the AGN near-IR case. In this respect, we note that the intercepts of the optical and near-IR R - L relationships are similar, a result which is not unexpected if the two AGN luminosities sample the canonical accretion disc spectrum ($f_{\nu} \propto \nu^{1/3}$). In this case, the difference in integrated luminosity would be ~ 0.4 dex, well within the scatter of ~ 0.5 dex of the near-IR and optical relationships for our sample (see Table 2). Fig. 2 further illustrates the efficacy of our approach to minimising the host-galaxy contamination of the near-IR AGN continuum. While the near-IR luminosities we measure correlate well with the measured optical luminosities (open circles), with a slope of 0.91 ± 0.04 , they correlate even better once the host-galaxy contributions to the optical luminosities have been removed. The slope of the

Table 2. Best-Fits for the Relation $\log R_{H\beta} = K + \alpha \log(\nu L_{\nu}/10^{43})$

| $\nu L_{1\mu\text{m}}$ (14 obj.) | | | $\nu L_{1\mu\text{m}}^{\text{AGN}}$ (14 obj.) | | | $\nu L_{5100\text{\AA}}^{\text{AGN}}$ (14 obj.) | | | $\nu L_{5100\text{\AA}}^{\text{AGN}}$ (34 obj.) | | | |
|----------------------------------|-----------|--|---|--|--|---|-----------|--|---|--|-----------|------|
| Type | K | α | S* | K | α | S* | K | α | S* | K | α | S* |
| BCES | | | | | | | | | | | | |
| Avg | 0.91±0.11 | 0.56±0.10 | | 1.02±0.09 | 0.55±0.10 | | 0.91±0.12 | 0.56±0.12 | | 1.01±0.07 | 0.52±0.05 | |
| MC | 0.90±0.13 | 0.56 ^{+0.12} _{-0.14} | | 1.01 ^{+0.11} _{-0.12} | 0.55 ^{+0.11} _{-0.13} | | 0.91±0.14 | 0.56±0.13 | | 0.98±0.10 | 0.52±0.07 | |
| FITEXY | | | | | | | | | | | | |
| Avg | 0.82±0.10 | 0.52±0.10 | 53 | 0.95±0.08 | 0.52±0.08 | 48 | 0.84±0.09 | 0.53±0.10 | 50 | 0.91±0.06 | 0.54±0.05 | 40 |
| MC | 0.81±0.11 | 0.53±0.11 | 52±2 | 0.93±0.09 | 0.52±0.09 | 48±2 | 0.82±0.11 | 0.53 ^{+0.10} _{-0.11} | 51±2 | 0.90 ^{+0.08} _{-0.07} | 0.54±0.06 | 41±1 |
| GaussFit | | | | | | | | | | | | |
| Avg | 1.00±0.10 | 0.54±0.10 | | 1.09±0.08 | 0.54±0.09 | | 0.97±0.09 | 0.56±0.09 | | 1.01±0.05 | 0.53±0.04 | |
| MC | 0.95±0.14 | 0.56±0.12 | | 1.07±0.11 | 0.54 ^{+0.09} _{-0.10} | | 0.92±0.12 | 0.58±0.10 | | 0.96±0.08 | 0.56±0.05 | |

* Scatter calculated as the percentage of the $\log R_{H\beta}$ value that, when added in quadrature to the error value, gives $\chi^2_{\nu} = 1$

relationship between the optical AGN luminosities and the near-IR luminosities is 1.03 ± 0.07 . Clearly the narrow-slit near-IR luminosities are dominated by the AGN component.

As we noted earlier, attenuation by dust is much reduced in the near-IR compared to the optical, so the $1\ \mu\text{m}$ continuum luminosity may be particularly useful as an alternative for dust-obscured AGN. A modest intrinsic obscuration of a hydrogen column density of $N_{\text{H}} \sim 10^{22}\ \text{cm}^{-2}$ results in a flux attenuation a factor of ~ 40 smaller at $1\ \mu\text{m}$ than at $5100\ \text{\AA}$ (in the rest-frame). The case is even more extreme for Compton-thick AGN with their expected hydrogen column densities in excess of $N_{\text{H}} \gtrsim 10^{24}\ \text{cm}^{-2}$ (e.g., Daddi et al. 2007).

As we have shown in Landt et al. (2011), AGN black holes masses can be estimated from the near-IR virial product based on the $1\ \mu\text{m}$ continuum luminosity and the width of the $\text{Pa}\beta$ (or $\text{Pa}\alpha$) broad emission line because the widths of the broad Paschen lines are well-correlated with those of the broad Balmer lines (Landt et al. 2008). The advantages of using the near-IR instead of the optical virial product are threefold. First, since $\text{Pa}\alpha$ and $\text{Pa}\beta$ are observed to be unblended (Landt et al. 2008), their width can be reliably measured. By contrast, the $\text{H}\beta$ broad emission line is generally observed to be strongly blended with both Fe II and He II $\lambda 4686$ and often shows a “red shelf” most likely formed by weak Fe II multiplets and He I. Secondly, the AGN continuum around $1\ \mu\text{m}$ is free from major contaminating components and may be easily determined, unlike the optical, which can suffer from an Fe II pseudo-continuum. Finally, since the near-IR is much less affected by dust extinction, it can potentially be applied to dust-obscured AGN.

4 CONCLUSIONS

We have presented the near-IR radius–luminosity relationship. Using near-IR spectra of 14 reverberation-mapped AGN obtained through a slit small enough that it excludes most of the host galaxy starlight, we have fit the relationship between the radius of the $\text{H}\beta$ broad-emission line region and the integrated $1\ \mu\text{m}$ continuum luminosity. The best-fit slope is in most cases $\sim 0.5 \pm 0.1$ and always consistent

with a value of 0.5, which is expected based on simple photoionisation arguments. The near-IR R – L relationship as an alternative to the optical relationship is expected to be relevant particularly for dust-obscured AGN. Black hole mass estimates can be obtained from the near-IR virial product based on the integrated $1\ \mu\text{m}$ continuum luminosity and the widths of the strong and unblended Paschen broad emission lines $\text{Pa}\alpha$ or $\text{Pa}\beta$.

ACKNOWLEDGMENTS

We thank the anonymous referee for comments that helped us to improve the paper. B. M. P. acknowledges support by the National Science Foundation (NSF grant no. AST-1008882). This research has made use of the NASA/IPAC Extragalactic Database (NED), which is operated by the Jet Propulsion Laboratory, California Institute of Technology, under contract with the National Aeronautics Space Administration.

REFERENCES

- Akritas, M. G., & Bershad, M. A. 1996, *ApJ*, 470, 706
- Bentz, M. C., Peterson, B. M., Netzer, H., Pogge, R. W., & Vestergaard, M. 2009, *ApJ*, 697, 160
- Bentz, M. C., Peterson, B. M., Pogge, R. W., Vestergaard, M., & Onken, C. A. 2006, *ApJ*, 644, 133
- Daddi, E., et al. 2007, *ApJ*, 670, 173
- Dasyra, K. M., et al. 2008, *ApJ*, 674, L9
- Denney, K. D., et al. 2010, *ApJ*, 721, 715
- Ferrarese, L., & Merritt, D. 2000, *ApJ*, 539, L9
- Gebhardt, K., et al. 2000, *ApJ*, 539, L13
- Greene, J. E., et al. 2010, *ApJ*, 723, 409
- Heckman, T. M., Kauffmann, G., Brinchmann, J., Charlot, S., Tremonti, C., & White, S. D. M. 2004, *ApJ*, 613, 109
- Kaspi, S., Maoz, D., Netzer, H., Peterson, B. M., Vestergaard, M., & Jannuzi, B. T. 2005, *ApJ*, 629, 61
- Kaspi, S., Smith, P. S., Netzer, H., Maoz, D., Jannuzi, B. T., & Givon, U. 2000, *ApJ*, 533, 631

- Kelly, B. C., Vestergaard, M., & Fan, X. 2009, *ApJ*, 692, 1388
- Kim, D., Im, M., & Kim, M. 2010, *ApJ*, 724, 386
- Landt, H., Bentz, M. C., Ward, M. J., Elvis, M., Peterson, B. M., Korista, K. T., & Karovska, M. 2008, *ApJS*, 174, 282
- Landt, H., Elvis, M., Ward, M. J., Bentz, M. C., Korista, K. T., & Karovska, M. 2011, arXiv:1101.3342
- Magorrian, J., et al. 1998, *AJ*, 115, 2285
- McArthur, B., Jefferys, W., & McCartney, J. 1994, in *Bulletin of the American Astronomical Society*, Vol. 26, 900
- Peterson, B. M. 1993, *PASP*, 105, 247
- Peterson, B. M., et al. 2004, *ApJ*, 613, 682
- Press, W. H., Teukolsky, S. A., Vetterling, W. T., & Flannery, B. P. 2007, *Numerical Recipes 3rd Edition: The Art of Scientific Computing* (Cambridge University Press)
- Rayner, J. T., Toomey, D. W., Onaka, P. M., Denault, A. J., Stahlberger, W. E., Vacca, W. D., Cushing, M. C., & Wang, S. 2003, *PASP*, 115, 362
- Tremaine, S., et al. 2002, *ApJ*, 574, 740
- Wandel, A., Peterson, B. M., & Malkan, M. A. 1999, *ApJ*, 526, 579
- Yu, Q., & Tremaine, S. 2002, *MNRAS*, 335, 965

This paper has been typeset from a $\mathrm{T}_{\mathrm{E}}\mathrm{X}/\mathrm{L}^{\mathrm{A}}\mathrm{T}_{\mathrm{E}}\mathrm{X}$ file prepared by the author.